Electron-phonon scattering dynamics in ferromagnetic metals and their influence on ultrafast demagnetization processes

Sven Essert and Hans Christian Schneider[*]

Department of Physics and Research Center OPTIMAS, University of Kaiserslautern, P.O. Box 3094, D-67653 Kaiserslautern, Germany
(Received 22 August 2011; published 9 December 2011)

We theoretically investigate spin-dependent carrier dynamics due to the electron-phonon interaction after ultrafast optical excitation in ferromagnetic metals. We calculate the electron-phonon matrix elements including the spin-orbit interaction in the electronic wave functions and the interaction potential. Using the matrix elements in Boltzmann scattering integrals, the momentum-resolved carrier distributions are obtained by solving their equation of motion numerically. We find that the optical excitation with realistic laser intensities alone leads to a negligible magnetization change, and that the demagnetization due to electron-phonon interaction is mostly due to hole scattering. Importantly, the calculated demagnetization quenching due to this Elliot-Yafet-type depolarization mechanism is not large enough to explain the experimentally observed result. We argue that the ultrafast demagnetization of ferromagnets does not occur exclusively via an Elliott-Yafet type process, i.e., scattering in the presence of the spin-orbit interaction, but is influenced to a large degree by a dynamical change of the band structure, i.e., the exchange splitting.

I. INTRODUCTION

It was first demonstrated more than ten years ago that the magnetization of ferromagnets can be "quenched" on ultrashort time scales after ultrafast optical excitation.[1] Apart from the possibilities for the ultrafast manipulation of ferromagnetism in applications, this observation raised the question of how demagnetization dynamics in ferromagnets on a time scale of a few hundred femtoseconds can be understood.

Aside from the phenomenological three-temperature model,[1,2] which leads to quite successful comparison with experiment, there are several theoretical models and experimental results that try to explain aspects of the underlying microscopic dynamics. For instance, the analysis of x-ray magnetic circular dichroism measurements suggested that the orbital magnetic moment does not play a prominent role in the demagnetization dynamics.[3,4] The authors of Ref. 3 concluded that an ultrafast spin-lattice coupling should be operative to explain the results. It has also been argued based on experimental results[5] that the excitation of magnons should play an important role. On the theory side, magnetic switching due to electronic transitions during the duration of a pump laser pulse has been analyzed in ferromagnets[6,7] as well as in oxides (including phonons),[8] and the Landau-Lifshitz-Bloch equations have been used to describe the magnetic dynamics.[9]

Perhaps the most popular microscopic explanations of the effect involve variations of the so-called Elliott-Yafet mechanism, in which demagnetization (or depolarization in semiconductors) is due to incoherent scattering of carriers between states that are spin-mixed due to the spin-orbit interaction. Electron-electron scattering is a possible candidate as the underlying scattering mechanism,[10,11] but the focus is usually on the effects of electron-phonon scattering in quasiequilibrium.[12–16] In addition, superdiffusive transport processes can contribute to the measured Kerr-effect signal because minority and majority electrons may simply leave the probe area at different speeds.[17]

In our opinion, it has so far been impossible rule out a single one of these mechanisms, let alone to pinpoint the dominant one. As a first step in this direction, we analyze a parameter-free microscopic model for ultrafast demagnetization and compare it with experiment. To keep things simple while allowing a conclusive statement, we exclusively treat the effect of the optical excitation and electron-phonon scattering at the level of Boltzmann scattering integrals while neglecting dynamical changes in the band structure, i.e., the exchange splitting, in the course of the dynamics. We evaluate the model using *ab initio* results for the simple ferromagnets nickel and iron. Comparison of the results of the present paper with experimental data, which are available from many different measurements, will show that a model without band structure changes yields a demagnetization that is too small.

This paper is organized as follows. In Sec. II we present the dynamical equations for the carrier distribution functions and show how we calculate the electron-phonon and dipole matrix elements using a first-principles approach. In Sec. III we discuss the numerical results of this model and show that the demagnetization using realistic parameters for the ultrashort-pulse excitation is due to hole dynamics, but too small to agree with experiment. A qualitative consideration shows that this conclusion should not be altered by including additional scattering processes. Section IV contains the conclusions and the Appendix describes details of our numerical evaluation of the dynamical equations.

II. THEORY

A. Dynamical equations

The basic idea of this paper is to integrate the dynamical equations of motion for the band- and momentum-resolved carrier distributions $n_{\vec{k}}^{\mu}(t)$. Our model includes the incoherent scattering dynamics due to the electron-phonon interaction, as well as the optical excitation, so that the general form of the dynamical equation is

$$\frac{\partial}{\partial t} n_{\vec{k}}^{\mu} = \frac{\partial}{\partial t} n_{\vec{k}}^{\mu} \Big|_{\text{opt}} + \frac{\partial}{\partial t} n_{\vec{k}}^{\mu} \Big|_{\text{e-p}}. \tag{1}$$

The optical excitation is given by

$$\frac{\partial}{\partial t} n_{\vec{k}}^{\mu}\Big|_{\text{opt}} = \frac{2\pi}{\hbar} \sum_{\nu(\neq\mu)} |\vec{d}_{\vec{k}}^{\mu\nu} \cdot \vec{E}(t)|^2 g(\epsilon_{\vec{k}}^{\mu} - \epsilon_{\vec{k}}^{\nu} - \hbar\omega_L)$$
$$\times [n_{\vec{k}}^{\nu} - n_{\vec{k}}^{\mu}]. \qquad (2)$$

Here, $\epsilon_{\vec{k}}^{\mu}$ is the energy of a carrier in a single-particle state $\psi_{\vec{k}}^{\mu}$ with band index μ and momentum $\vec{k}$. The dipole matrix element for a transition connecting two such states is denoted by $\vec{d}_{\vec{k}}^{\mu\nu} = \langle \psi_{\vec{k}}^{\mu} | e\vec{r} | \psi_{\vec{k}}^{\nu} \rangle$. The optical excitation is characterized by the dynamical electric-field amplitude $\vec{E}(t)$, a central laser frequency ω_L, and the function $g(\epsilon)$ that includes the spectral profile of the laser pulse.

The electron-phonon contribution to the carrier dynamics at the level of Boltzmann scattering integrals reads

$$\frac{\partial}{\partial t} n_{\vec{k}}^{\mu}\Big|_{\text{e-p}} = \frac{2\pi}{\hbar} \sum_{\vec{k}',\nu} \big[w(\vec{k}',\nu \to \vec{k},\mu) n_{\vec{k}'}^{\nu} (1 - n_{\vec{k}}^{\mu})$$
$$- w(\vec{k},\mu \to \vec{k}',\nu) n_{\vec{k}}^{\mu} (1 - n_{\vec{k}'}^{\nu}) \big], \qquad (3)$$

where the scattering rates $w(\vec{k}',\nu \to \vec{k},\mu)$ from state $\psi_{\vec{k}'}^{\nu}$ to $\psi_{\vec{k}}^{\mu}$,

$$w(\vec{k}',\nu \to \vec{k},\mu)$$
$$= \sum_{\lambda} \big[|M_{+}^{\vec{k}-\vec{k}',\lambda}(\vec{k}',\nu \to \vec{k},\mu)|^2 \tilde{n}_{\vec{k}-\vec{k}'}^{\lambda} \delta(\epsilon_{\vec{k}'}^{\nu} - \epsilon_{\vec{k}}^{\mu} + \hbar\omega_{\vec{k}-\vec{k}'}^{\lambda})$$
$$+ |M_{-}^{\vec{k}'-\vec{k},\lambda}(\vec{k}',\nu \to \vec{k},\mu)|^2 (\tilde{n}_{\vec{k}'-\vec{k}}^{\lambda} + 1)$$
$$\times \delta(\epsilon_{\vec{k}'}^{\nu} - \epsilon_{\vec{k}}^{\mu} - \hbar\omega_{\vec{k}'-\vec{k}}^{\lambda}) \big], \qquad (4)$$

have contributions from absorption ("+") and emission ("−") processes. The (angular) frequency of a phonon mode λ is designated by $\omega_{\vec{q}}^{\lambda}$ and its occupation at quasimomentum $\vec{q}$ by $\tilde{n}_{\vec{q}}^{\lambda}$. The electron-phonon interaction matrix elements $M_{\pm}^{\vec{q},\lambda}(\vec{k}',\nu \to \vec{k},\mu)$ result from the change of the electron-lattice interaction energy due to the vibrational motion of the nuclei. For small displacements they are given by

$$M_{\pm}^{\vec{q},\lambda}(\vec{k}',\nu \to \vec{k},\mu) = \sqrt{\frac{\hbar}{2MN\omega_{\vec{q}}^{\lambda}}} \sum_{j} e^{\pm i\vec{q}\cdot\vec{R}_j}$$
$$\times \langle \psi_{\vec{k}}^{\mu} | \vec{\pi}_{\vec{q}}^{\lambda} \cdot \frac{\partial}{\partial \vec{R}_j} V(\vec{r}; \{\vec{R}_i\}) | \psi_{\vec{k}'}^{\nu} \rangle. \quad (5)$$

The electron-lattice interaction potential $V(\vec{r}; \{\vec{R}_i\})$ depends on the electron position $\vec{r}$ and, in principle, on the set of the positions of the nuclei $\{\vec{R}_i\}$ in the crystal composed of N unit cells with atomic mass M. The polarization vector of the phonon mode $(\vec{q},\lambda)$ is denoted by $\vec{\pi}_{\vec{q}}^{\lambda}$. The upper and lower signs in the exponential are associated with the phonon absorption $M_{+}^{\vec{q},\lambda}(\vec{k}',\nu \to \vec{k},\mu)$ and emission $M_{-}^{\vec{q},\lambda}(\vec{k}',\nu \to \vec{k},\mu)$ matrix elements, respectively.

In our calculation, we assume that the phonon occupation numbers are time independent and remain at their equilibrium values,

$$\tilde{n}_{\vec{q}}^{\lambda} = \frac{1}{e^{\hbar\omega_{\vec{q}}^{\lambda}/k_B T_0} - 1}. \qquad (6)$$

This amounts to a bath assumption for the phonon system, and in this paper we fix its temperature at $T_0 = 300$ K, i.e., the temperature of the unexcited system in most studies of demagnetization dynamics.

From the dynamical electronic occupation numbers calculated according to Eq. (1), we obtain the time-dependent magnetization by

$$M(t) = \frac{2\mu_B}{\hbar} \sum_{\vec{k}} \sum_{\mu} \langle S_z \rangle_{\vec{k}}^{\mu} n_{\vec{k}}^{\mu}(t), \qquad (7)$$

with the single-particle spin expectation value

$$\langle S_z \rangle_{\vec{k}}^{\mu} = \langle \psi_{\vec{k}}^{\mu} | \hat{S}_z | \psi_{\vec{k}}^{\mu} \rangle \qquad (8)$$

in the Bloch state $|\psi_{\vec{k}}^{\mu}\rangle$ and the Bohr magneton μ_B. In writing these relations, we have chosen the z direction as the direction of the ferromagnetic polarization. Orbital angular-momentum contributions to the magnetization are neglected in Eq. (7). Although the orbital contribution to the magnetization is quenched in the ground state of a $3d$ ferromagnet, it is not clear whether this carries over to the dynamics in excited states as computed here. The paper by Carva *et al.*[4] suggests that the XMCD sum rules for spin and orbital magnetic moments remain valid, at least under the nonequilibrium conditions assumed in that paper. This provides an indication that the orbital contribution to the magnetization of $3d$ ferromagnets is not increased dramatically under laser-excitation conditions

B. Electron-phonon matrix elements

The numerical evaluation of Eq. (1) requires as input material properties, in particular, the electronic band structure $\epsilon_{\vec{k}}^{\mu}$, the spin expectation value of the single-particle states $\langle S_z \rangle_{\vec{k}}^{\mu}$, the dipole-transition matrix elements $\vec{d}_{\vec{k}}^{\mu\nu}$, the phonon dispersion $\omega_{\vec{q}}^{\lambda}$, and, importantly, the electron-phonon matrix elements $M_{\pm}^{\vec{q},\lambda}(\vec{k}',\nu \to \vec{k},\mu)$. We obtain these quantities from density-functional theory to avoid the introduction of adjustable parameters. To this end, we employ the augmented spherical wave (ASW) method[18] as described in the monograph Ref. [19] (see also Ref. [20]). The implementation of the ASW method used by us was developed in the Kübler group and relies on the scalar relativistic and local spin-density approximations. It includes spin-orbit coupling in a second variational correction.

The starting point for the calculation of the matrix elements is the representation of the wave function of a single-particle state with band index μ and momentum $\vec{k}$ in the ASW basis. Since we employ the *atomic sphere approximation* (ASA) it is usually sufficient to know the wave functions inside the atomic spheres where they are given by

$$\psi_{\vec{k}}^{\mu}(\vec{r}) = \sum_{L,\sigma} \big[C_{L\sigma}^{\mu}(\vec{k}) i^l \tilde{h}_{l\sigma}(r) + A_{L\sigma}^{\mu}(\vec{k}) i^l \tilde{j}_{l\sigma}(r) \big] Y_L(\hat{r}) \chi_{\sigma}, \quad (9)$$

where $\tilde{h}_{l\sigma}(r)$ and $\tilde{j}_{l\sigma}(r)$ are *augmented spherical waves*, $Y_L(\hat{r})$ spherical harmonics, and χ_{σ} Pauli spinors. Here, $L = (l,m)$ is a multiindex that includes both the angular momentum and the magnetic quantum number. The relatively simple expression given here is only valid for materials with a basis consisting of a single atom, such as the simple ferromagnets investigated

in the present paper. The augmented spherical waves, together with the coefficients $A_{L\sigma}^{\mu}(\vec{k})$ and $C_{L\sigma}^{\mu}(\vec{k})$, are calculated self-consistently during the iterative solution of the Kohn-Sham equations.

For the evaluation of Eq. (5), we employ the so-called *rigid-ion approximation*. That is, we assume that we can write the lattice-configuration dependence of the electron-phonon interaction potential,

$$V(\vec{r}; \{\vec{R}_i\}) = \sum_i v(\vec{r} - \vec{R}_i), \tag{10}$$

as a superposition of the on-site potentials $v(\vec{r})$; see below, Eq. (12). We also assume that the potential v vanishes outside the atomic sphere. The rigid-ion approximation is known to give a quite realistic description of the electron-phonon coupling in transition metals.[21]

Equation (5) can then be simplified to yield

$$M_{\pm}^{\vec{q},\lambda}(\vec{k}',v \to \vec{k},\mu)$$
$$= -\sqrt{\frac{\hbar}{2MN\omega_{\vec{q}}^{\lambda}}} \delta_{\vec{k}'\pm\vec{q}-\vec{k},\vec{G}} \int_{\mathrm{UC}} d^3r\, \psi_{\vec{k}}^{\mu*}(\vec{r}) [\vec{\pi}_{\vec{q}}^{\lambda} \cdot \nabla v(\vec{r})]$$
$$\times \psi_{\vec{k}'}^{v}(\vec{r}), \tag{11}$$

where UC denotes an integral over the unit cell, which due to the ASA is assumed to be spherical. For the on-site potential experienced by the electrons, we include the spin-averaged radial Kohn-Sham potential $V_{\mathrm{eff}}(r)$ as well as the spin-orbit interaction

$$v(\vec{r}) = V_{\mathrm{eff}}(r) + \frac{\hbar}{(2mc)^2}\frac{1}{r}\frac{dV_{\mathrm{eff}}(r)}{dr}\vec{\sigma}\cdot(\vec{r}\times\vec{p}). \tag{12}$$

The additional spin-orbit term is often neglected for the electron-phonon interaction, even though it has been shown to be of importance for spin relaxation in materials with time-inversion symmetry.[22] Not much is known about the influence of this term in ferromagnets where the time-inversion symmetry is broken. We therefore calculate the matrix element with and without the spin-orbit contribution and show that our final results on ultrafast demagnetization are not qualitatively influenced by the inclusion of the second term.

We first give the result for the calculation *without* the spin-orbit contribution in Eq. (12). In this case we can directly evaluate the integral over the unit cell in Eq. (11):

$$\int_{\mathrm{UC}} d^3r\, \psi_{\vec{k}}^{\mu*}(\vec{r}) \nabla V_{\mathrm{eff}}(r) \psi_{\vec{k}'}^{v}(\vec{r})$$
$$= \int_{\mathrm{UC}} d^3r\, \psi_{\vec{k}}^{\mu*}(\vec{r}) \frac{dV_{\mathrm{eff}}(r)}{dr}\hat{r}\psi_{\vec{k}'}^{v}(\vec{r})$$
$$= \sum_{\sigma}\sum_{L,L'} \vec{G}_{LL'} \left[A_{L\sigma}^{\mu*}(\vec{k})A_{L'\sigma}^{v}(\vec{k}')\langle\tilde{j}|\frac{dV_{\mathrm{eff}}}{dr}|\tilde{j}\rangle_{l\sigma,l'\sigma}\right.$$
$$+ C_{L\sigma}^{\mu*}(\vec{k})A_{L'\sigma}^{v}(\vec{k}')\langle\tilde{h}|\frac{dV_{\mathrm{eff}}}{dr}|\tilde{j}\rangle_{l\sigma,l'\sigma}$$
$$+ A_{L\sigma}^{\mu*}(\vec{k})C_{L'\sigma}^{v}(\vec{k}')\langle\tilde{j}|\frac{dV_{\mathrm{eff}}}{dr}|\tilde{h}\rangle_{l\sigma,l'\sigma}$$
$$\left. + C_{L\sigma}^{\mu*}(\vec{k})C_{L'\sigma}^{v}(\vec{k}')\langle\tilde{h}|\frac{dV_{\mathrm{eff}}}{dr}|\tilde{h}\rangle_{l\sigma,l'\sigma} \right]. \tag{13}$$

The radial matrix elements

$$\langle\tilde{f}|\frac{dV_{\mathrm{eff}}}{dr}|\tilde{g}\rangle_{l\sigma,l'\sigma'}$$
$$= (-1)^l\, i^{l+l'} \int_0^{r_K} r^2 \tilde{f}_{l\sigma}(r)\frac{dV_{\mathrm{eff}}(r)}{dr}\tilde{g}_{l'\sigma'}(r)dr \tag{14}$$

can be calculated by integrating the gradient of the Kohn-Sham potential and

$$\vec{G}_{LL'} = \int d\Omega\, Y_L^*(\hat{r})\hat{r}Y_{L'}(\hat{r}) \tag{15}$$

can be evaluated in terms of Gaunt coefficients.[20]

The calculation of the electron-phonon interaction matrix element (11) *including the spin-orbit contribution* could, in principle, be achieved by evaluating the integral

$$\int_{\mathrm{UC}} d^3r\, \psi_{\vec{k}}^{\mu*}(\vec{r})\nabla\left[\frac{\hbar}{(2mc)^2}\frac{1}{r}\frac{dV_{\mathrm{eff}}(r)}{dr}\vec{\sigma}\cdot(\vec{r}\times\vec{p})\right]\psi_{\vec{k}'}^{v}(\vec{r}) \tag{16}$$

and adding it to Eq. (13). However, straightforward numerical evaluation of Eq. (16) runs into difficulties because of the strong divergence of the integrand for $r \to 0$. We circumvent this problem by calculating the complete matrix element (11) by rewriting the gradient of the potential including the spin-orbit interaction [Eq. (12)] as a commutator,

$$\nabla v(\vec{r}) = \frac{i}{\hbar}[\vec{p}, H_{\mathrm{eff}}], \tag{17}$$

with the Hamiltonian $H_{\mathrm{eff}} = \frac{p^2}{2m} + v(\vec{r})$. For the evaluation of matrix elements of H_{eff}, we will assume that it produces the energy eigenvalues $\epsilon_{\vec{k}}^{\mu}$ when acting on the corresponding Kohn-Sham eigenvector, even though the eigenenergies and eigenvectors are computed using scalar relativistic corrections to H_{eff}. If we now assume completeness of the ASW basis, Eq. (17) may be used for a reformulation in terms of the momentum matrix elements,

$$\int_{\mathrm{UC}} d^3r\, \psi_{\vec{k}}^{\mu*}(\vec{r})\nabla v(\vec{r})\psi_{\vec{k}'}^{v}(\vec{r})$$
$$= \frac{i}{\hbar}\int_{\mathrm{UC}} d^3r\, \psi_{\vec{k}}^{\mu*}(\vec{r})[\vec{p}\,H_{\mathrm{eff}} - H_{\mathrm{eff}}\,\vec{p}]\psi_{\vec{k}'}^{v}(\vec{r}) \tag{18}$$
$$= \frac{i}{\hbar}\epsilon_{\vec{k}'}^{v}\langle\psi_{\vec{k}}^{\mu}|\vec{p}|\psi_{\vec{k}'}^{v}\rangle_{\mathrm{UC}} - \frac{i}{\hbar}\sum_{\eta}\epsilon_{\vec{k}'}^{\eta}\langle\psi_{\vec{k}}^{\mu}|\psi_{\vec{k}'}^{\eta}\rangle_{\mathrm{UC}}\langle\psi_{\vec{k}'}^{\eta}|\vec{p}|\psi_{\vec{k}'}^{v}\rangle_{\mathrm{UC}},$$
$$\tag{19}$$

where the momentum matrix elements $\langle\psi_{\vec{k}}^{\mu}|\vec{p}|\psi_{\vec{k}'}^{v}\rangle_{\mathrm{UC}}$ are calculated in the ASA using a consistent method developed by Oppeneer *et al.*[23] Since $\nabla v(\vec{r})$ is a Hermitian operator on the unit cell, we can derive the following expression that is more symmetric with regard to initial and final states:

$$\int_{\mathrm{UC}} d^3r\, \psi_{\vec{k}}^{\mu*}(\vec{r})\nabla v(\vec{r})\psi_{\vec{k}'}^{v}(\vec{r})$$
$$= \frac{i}{2\hbar}\left[\int_{\mathrm{UC}} d^3r\, \psi_{\vec{k}}^{\mu*}(\vec{r})[\vec{p}\,H_{\mathrm{eff}} - H_{\mathrm{eff}}\,\vec{p}]\psi_{\vec{k}'}^{v}(\vec{r})\right.$$
$$\left. + \left(\int_{\mathrm{UC}} d^3r\, \psi_{\vec{k}'}^{v*}(\vec{r})[\vec{p}\,H_{\mathrm{eff}} - H_{\mathrm{eff}}\,\vec{p}]\psi_{\vec{k}}^{\mu}(\vec{r})\right)^*\right]$$

$$= \frac{i}{2\hbar} \Big[\epsilon_{\vec{k}'}^{\nu} \langle \psi_{\vec{k}}^{\mu} | \vec{p} | \psi_{\vec{k}'}^{\nu} \rangle_{\mathrm{UC}} + \epsilon_{\vec{k}}^{\mu} \langle \psi_{\vec{k}}^{\nu} | \vec{p} | \psi_{\vec{k}}^{\mu} \rangle_{\mathrm{UC}}^{*}$$

$$- \sum_{\eta} \epsilon_{\vec{k}'}^{\eta} \langle \psi_{\vec{k}}^{\mu} | \psi_{\vec{k}'}^{\eta} \rangle_{\mathrm{UC}} \langle \psi_{\vec{k}'}^{\eta} | \vec{p} | \psi_{\vec{k}'}^{\nu} \rangle_{\mathrm{UC}}$$

$$- \sum_{\eta} \epsilon_{\vec{k}}^{\eta} \langle \psi_{\vec{k}'}^{\nu} | \psi_{\vec{k}}^{\eta} \rangle_{\mathrm{UC}}^{*} \langle \psi_{\vec{k}}^{\eta} | \vec{p} | \psi_{\vec{k}}^{\mu} \rangle_{\mathrm{UC}}^{*} \Big]. \qquad (20)$$

Although our assumption of completeness may yield the matrix element only with a certain error because the ASW method uses a rather small number of basis functions, the qualitative conclusions discussed in the next section are not affected by this.

In the numerical calculations, we typically used a $\vec{k}$-point grid of about 2000 points in the irreducible wedge of the band structure, and the dynamical equations were solved on the same grid (see the Appendix for details on the numerical method). Experimental values for the lattice constants[24] were used. The phonon dispersion was calculated with QUANTUM ESPRESSO[25] in the same way as by Dal Corso *et al.*[26] The latter paper shows that phonon dispersions obtained in this approach are in good agreement with experimental data.

C. Dipole matrix elements

The dipole matrix elements are calculated by reformulating them in terms of the momentum matrix elements,

$$\vec{d}_{\vec{k}}^{\mu\nu} = \langle \psi_{\vec{k}}^{\mu} | e\vec{r} | \psi_{\vec{k}}^{\nu} \rangle$$

$$= \frac{ie\hbar}{m(\epsilon_{\vec{k}}^{\nu} - \epsilon_{\vec{k}}^{\mu})} \langle \psi_{\vec{k}}^{\mu} | \vec{p} + \frac{\hbar}{4mc^2}(\vec{\sigma} \times \nabla V_{\mathrm{eff}}(r)) | \psi_{\vec{k}}^{\nu} \rangle, \qquad (21)$$

where the momentum matrix elements $\langle \psi_{\vec{k}}^{\mu} | \vec{p} | \psi_{\vec{k}}^{\nu} \rangle$ are again calculated according to Oppeneer *et al.*[23] The contribution of the spin-orbit interaction is usually neglected. We include it here as it may directly contribute to spin flips, even though our numerical results in the end will show that the difference is insignificant. It can be calculated from the wave functions as follows:

$$\langle \psi_{\vec{k}}^{\mu} | (\vec{\sigma} \times \nabla V_{\mathrm{eff}}(r)) | \psi_{\vec{k}}^{\nu} \rangle$$

$$= \int_{\mathrm{UC}} d^3r \, \psi_{\vec{k}}^{\mu*}(\vec{r}) (\vec{\sigma} \times \hat{r}) \frac{dV_{\mathrm{eff}}(r)}{dr} \psi_{\vec{k}'}^{\nu}(\vec{r})$$

$$= \sum_{\sigma,\sigma'} \sum_{L,L'} \Big[(\chi_{\sigma}^{T} \vec{\sigma} \chi_{\sigma'}) \times \vec{G}_{LL'} \Big] \Big[A_{L\sigma}^{\mu*}(\vec{k}) A_{L'\sigma'}^{\nu}(\vec{k}') \langle \tilde{j} |$$

$$\times \frac{dV_{\mathrm{eff}}}{dr} | \tilde{j} \rangle_{l\sigma,l'\sigma'} + C_{L\sigma}^{\mu*}(\vec{k}) A_{L'\sigma'}^{\nu}(\vec{k}') \langle \tilde{h} | \frac{dV_{\mathrm{eff}}}{dr} | \tilde{j} \rangle_{l\sigma,l'\sigma'}$$

$$+ A_{L\sigma}^{\mu*}(\vec{k}) C_{L'\sigma'}^{\nu}(\vec{k}') \langle \tilde{j} | \frac{dV_{\mathrm{eff}}}{dr} | \tilde{h} \rangle_{l\sigma,l'\sigma'}$$

$$+ C_{L\sigma}^{\mu*}(\vec{k}) C_{L'\sigma'}^{\nu}(\vec{k}') \langle \tilde{h} | \frac{dV_{\mathrm{eff}}}{dr} | \tilde{h} \rangle_{l\sigma,l'\sigma'} \Big]; \qquad (22)$$

cf. Eq. (14) for the definition of the matrix elements involving V_{eff}.

III. RESULTS

In this section, we present numerical results obtained from the solution of the dynamical equation (1) and some qualitative considerations on the role of scattering processes in ultrafast demagnetization dynamics. For the calculations we use matrix elements computed as described in the previous sections. Further details of our numerical implementation of the dynamics are included in the Appendix.

A. Optical excitation

We first examine the excitation process by the ultrashort optical pulse without including the electron-phonon interaction. We model a homogeneous excitation of a ferromagnetic metal by a laser pulse with Gaussian temporal shape, full width at half maximum of 50 fs, and a spectral width of 100 meV at a central photon energy of $\hbar\omega_L = 1.55$ eV. These parameters, as well as the pulse intensity of 4 mJ/cm^2, are chosen to match typical experimental excitation conditions. To determine the electric-field amplitude present in the material we note that the chosen intensity corresponds to an electric-field amplitude of $E_0 = 7.5 \times 10^8$ V/m in vacuum. Reflection at the surface as well as the optical density of the material lead to a reduction of the field amplitude in the material,

$$E_0' = E_0 \frac{2}{\sqrt{(1+n)^2 + \kappa^2}}, \qquad (23)$$

where n and κ denote the real and the imaginary part of the refractive index, respectively. Taking $n = 2.22$, $\kappa = 4.90$ for nickel and $n = 2.92$, $\kappa = 3.36$ for iron, this leaves us with an amplitude in the material E_0' of 2.6×10^8 V/m for nickel and 2.9×10^8 V/m for iron.[27] We take these values of the field amplitude as constant throughout the sample for the calculation and neglect the attenuation due to absorption in the material as well as additional reflection/absorption due to oxide and protection layers. We therefore overestimate the field amplitude present in samples used for the experimental determination of the magnetization dynamics.

The optical excitation contribution alone, i.e., the first term on the right hand side of dynamical equation (1), leads to the magnetization dynamics shown in Fig. 1. This result should be compared to experimental values for a pulse energy density of 4 mJ/cm^2, such as those reported in Refs. 10 and 5 where a "quenching" of the magnetization down to 40% and 80% of the equilibrium magnetization was found for nickel and iron, respectively. It is clear from Fig. 1 that the magnetization change computed including only the incoherent optical excitation at the photon energy of 1.55 eV is orders of magnitude smaller than the one observed in experiment.

As a contribution to the magnetization change, the optical excitation is negligible, but it is still interesting to take a closer look at the carrier distributions created by the laser pulse because these are essentially the starting point of the momentum-resolved electron-phonon scattering dynamics. To this end, we analyze the energy-dependent occupation changes,

$$\Delta N_\sigma(\epsilon, t) = \sum_{\vec{k},\mu} \delta(\epsilon - \epsilon_{\vec{k}}^{\mu}) \langle \mathcal{P}_\sigma \rangle_{\vec{k}}^{\mu} [n_{\vec{k}}^{\mu}(t) - f(\epsilon_{\vec{k}}^{\mu}, T_0)], \qquad (24)$$
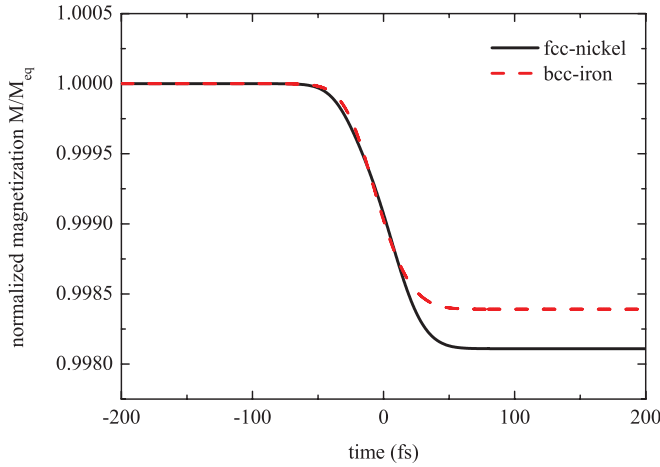
FIG. 1. (Color online) Magnetization dynamics due to optical excitation alone. The magnetization is normalized to its equilibrium value.

between the dynamical distributions $n_{\vec{k}}^{\mu}(t)$ compared to the equilibrium Fermi-Dirac functions $f(\epsilon_{\vec{k}}^{\mu}, T_0)$ that describe the carrier distributions in equilibrium at the sample temperature T_0 before the optical excitation. In Eq. (24) we separate occupation changes for minority and majority spins, i.e., for $\sigma = +$ and $-$, respectively, by projecting on the majority and minority spin contributions of the ASW wave functions using the spin-dependent weights (projections),

$$\langle \mathcal{P}_\sigma \rangle_{\vec{k}}^{\mu} = \sum_L \langle \psi_{\vec{k}}^{\mu} | \mathcal{P}_\sigma \psi_{\vec{k}}^{\mu} \rangle_L, \qquad (25)$$

of each state $\psi_{\vec{k}}^{\mu}$ where

$$\langle \psi_{\vec{k}}^{\mu} | \mathcal{P}_\sigma \psi_{\vec{k}}^{\nu} \rangle_L$$
$$= A_{L\sigma}^{\mu*}(\vec{k}) A_{L\sigma}^{\nu}(\vec{k}) \langle \tilde{j} | \tilde{j} \rangle_{l\sigma} + C_{L\sigma}^{\mu*}(\vec{k}) A_{L\sigma}^{\nu}(\vec{k}) \langle \tilde{h} | \tilde{j} \rangle_{l\sigma}$$
$$+ A_{L\sigma}^{\mu*}(\vec{k}) C_{L\sigma}^{\nu}(\vec{k}) \langle \tilde{j} | \tilde{h} \rangle_{l\sigma} + C_{L\sigma}^{\mu*}(\vec{k}) C_{L\sigma}^{\nu}(\vec{k}) \langle \tilde{h} | \tilde{h} \rangle_{l\sigma}. \quad (26)$$

The overlaps are given by

$$\langle \tilde{f} | \tilde{g} \rangle_{l\sigma} = \int_0^{r_K} r^2 \tilde{f}_{l\sigma}(r) \tilde{g}_{l\sigma}(r) dr. \qquad (27)$$

In this paper, we always use $T_0 = 300$ K as a starting point for the dynamical calculations to facilitate comparison with typical room-temperature measurements. Moreover, room temperature is still less than half the Curie temperature so that we can expect the exchange splitting to be not too different from its $T = 0$ K value, and therefore the DFT band structure should be a reasonable approximation.

Figures 2(b) and 2(c) show the spin- and energy-resolved occupation change, computed according to Eq. (24), due to optical excitation at times well after the pump pulse. It corresponds to the magnetization shown in Fig. 1 at 200 fs. In both materials, mainly minority carriers are excited. The pronounced negative and positive spikes in the minority-spin occupation changes are separated by the photon energy 1.55 eV and roughly coincide with maxima of the density of states [see Fig. 2(a)] for the minority carriers. These maxima stem from
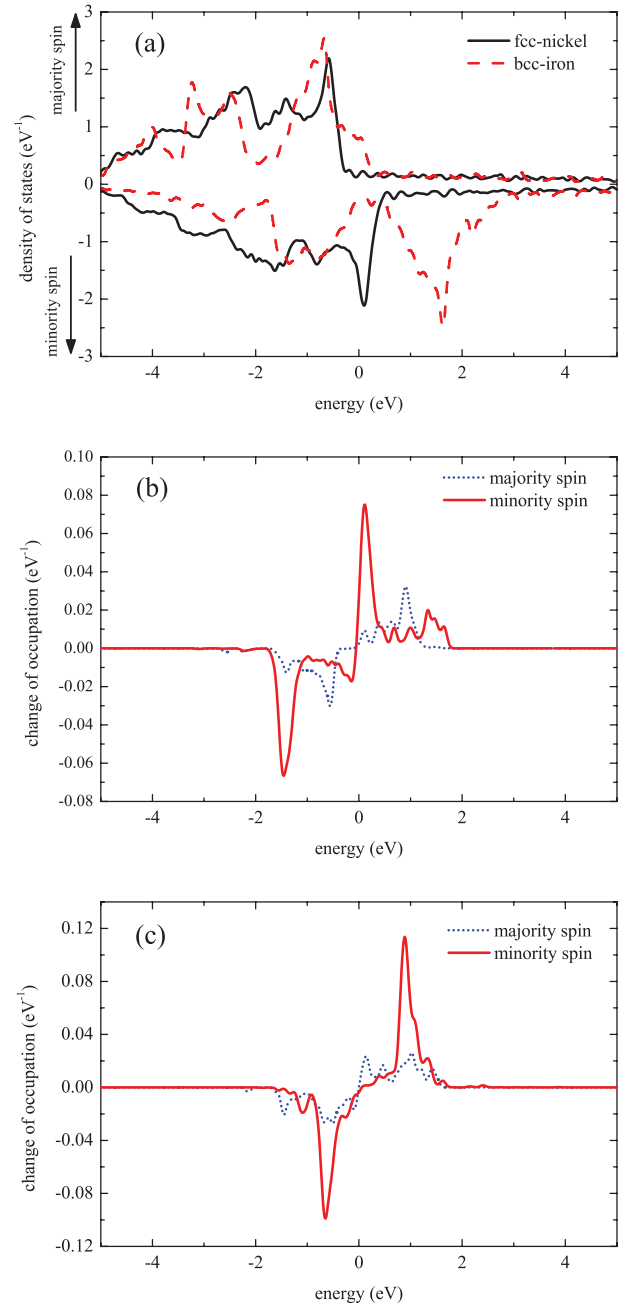

FIG. 2. (Color online) Spin-resolved density of states for nickel and iron (a) as well as energy- and spin-resolved occupation change after the optical excitation for nickel (b) and iron (c).

the d bands in these materials, which leads us to conclude that they play a major role in the optical excitation process.

The information about the distribution after the optical excitation contained in Figs. 2(b) and 2(c) allows one to draw conclusions about the maximal magnetization change achievable by electron-phonon scattering in our model, as this distribution is the starting point for the scattering dynamics. Electron-phonon scattering is a quasielastic process involving a single-electron, i.e., there is only a small amount of energy transferred in each scattering event. Due to the bath assumption for the phonon system in our calculation, there are also no "secondary electrons" excited because such a transfer of energy to

other electrons could only happen mediated by a phonon. We therefore expect that electron-phonon scattering will lead to a continuous relaxation of the excited carriers where the number of nonequilibrium electrons and holes decreases as they are scattered toward the Fermi energy. The demagnetization itself is caused by "spin-flip" scattering processes, i.e., scattering processes with different spin expectation values for initial and final wave functions, that occur during the relaxation process. Therefore the maximal demagnetization that can be caused by scattering in a fixed band structure occurs when all excited majority electrons and minority holes flip their spin while the minority electrons and majority holes do not undergo spin-flip scattering. The relative magnetization change in this physically rather unreasonable case is then given by

$$\max \frac{M}{M_{\text{eq}}} = \frac{\mu_{\text{eq}} - 2(N_-^{\text{e}} + N_+^{\text{h}})\mu_B}{\mu_{\text{eq}}}. \tag{28}$$

Here, μ_B is the Bohr magneton, and M_{eq} and μ_{eq} denote the equilibrium values of the material magnetization and of the magnetic moment per unit cell, respectively. The number of majority electrons N_-^{e} (minority holes N_+^{h}) per unit cell can be obtained from integrating the occupation changes in Fig. 2 above (below) the Fermi energy. With that estimate we find a minimal relative magnetization due to electron-phonon scattering of 0.84 in nickel and 0.94 in iron, which is a smaller demagnetization than observed in experiments. Without even calculating the full dynamics, we thus expect that microscopic electron-phonon scattering with a fixed band structure is not responsible for the pronounced drop of the magnetization observed in experiments.

We next take a closer look at the photon energy dependence of the excitation process. Fig. 3 shows the magnetization change M_∞/M_{eq} vs. the pump photon energy for a fixed electric-field amplitude of 2×10^8 V/m. For most of the pump photon energies between 0.1 and 4.5 eV the optical excitation leads to negligible demagnetization, as was discussed above in connection with Fig. 1 for a pump photon energy of 1.55 eV. Only at a pump photon energy of about 0.7 eV for nickel and 2.2 eV for iron one observes a magnetization change of significantly more than 1%, because these energies correspond to the exchange splitting of the d bands in these materials, so that absorption at these energies is likely to be associated with
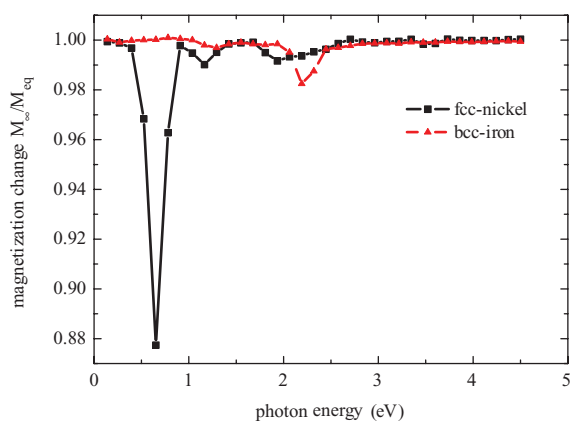
a change of carrier spin. The order of magnitude of our results for the achievable magnetization change by optical excitation alone seems to be in agreement with those of Zhang *et al.*[7] for the change of magnetization due to the coherent excitation by an optical pulse.

B. Electron-phonon scattering

In this section, we present results for the carrier dynamics including both optical excitation and electron-phonon scattering. We start by examining in Fig. 4 the magnetization dynamics and the time evolution of the energy in the electronic system for the same parameters that were used in Fig. 1 for the case of optical excitation only. Comparing the magnetization dynamics including electron-phonon scattering in Fig. 4 to those without, cf. Fig. 1, one notices an enhanced demagnetization of about 3–5%. Yet, this magnetization change is smaller than the estimate of the previous section. Due to the scattering, the dynamics now also include a relaxation to equilibrium. This can be made visible by monitoring the energy in the electronic system [Fig. 4(b)], which nicely shows the sudden energy transfer from the laser pulse and a subsequent almost exponential decay with time constants of about 2 ps for nickel and 2.5 ps for iron. These time constants are significantly longer than the electron-phonon coupling times obtained from the analysis of experimental data for these materials ranging from 0.3–0.5 ps.[5,12] Likely,
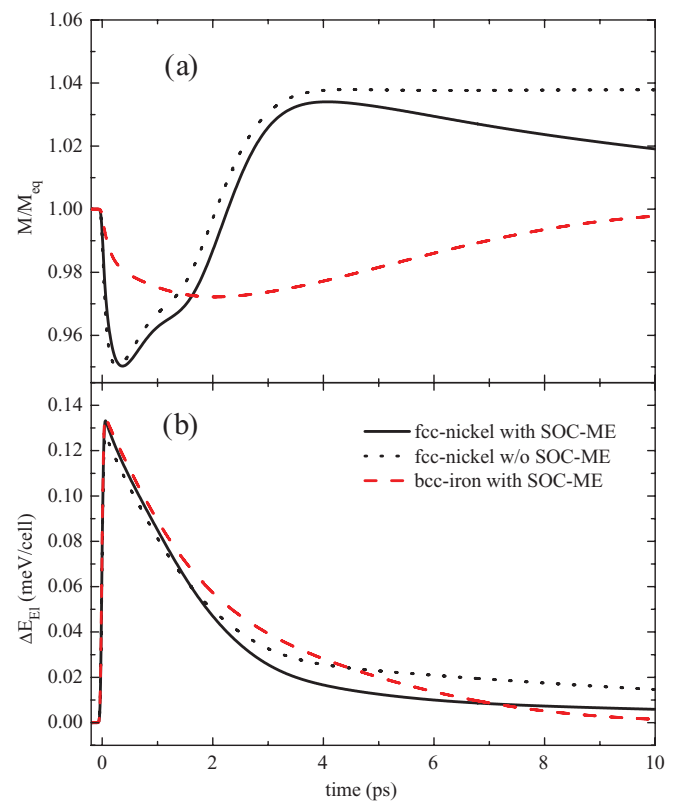
FIG. 4. (Color online) Normalized magnetization dynamics (a) and energy difference to equilibrium of the electronic system (b) after the optical excitation including electron-phonon scattering. Results obtained including the spin-orbit coupling contribution in the electron-phonon matrix element are labeled "with SOC-ME."

FIG. 3. (Color online) Magnetization change achievable by optical excitation alone for a range of pump-photon energies.

this is because we neglect other scattering mechanisms (such as electron-electron scattering), which open up additional scattering paths and lead to an overall speedup of the relaxation process. The magnetization for nickel even rises above its value at equilibrium, which is understandable because there is no fundamental law that prohibits nonequilibrium scattering dynamics from going through intermediate states with an increased magnetization. Whether these are reached depends on the band structure, the properties of the states involved, and the initial/excitation conditions.

When comparing the calculated magnetization dynamics to experimental results, one should keep in mind that our calculation neglects changes in the band structure, i.e., the exchange splitting, and the subsequent relaxation of these changes back into equilibrium. Processes associated with the change of the exchange splitting are expected to dominate the dynamics after a quasiequilibrium magnetization has been established, namely for times longer than about 5 ps.[28] A meaningful comparison with experiment of the present model should therefore be limited to a few picoseconds, which is the dynamical time scale for which the different microscopic models mentioned in the Introduction have been proposed. In that time window, we find that roughly the same results (which for clarity reasons are only shown for nickel in Fig. 4) are obtained if the spin-orbit term in the interaction matrix elements [cf. Eq. (12)] is neglected.

To get a better understanding of the demagnetization in the present model, it is instructive to look at the carrier distributions at different stages of the dynamics. We present only the results for nickel in this paper, as the carrier dynamics in iron shows similar behavior. In Fig. 5 we plot the energy- and spin-resolved occupation change at different times. Note that after the end of the optical excitation at about 50 fs the excited carrier density above the Fermi energy (at 0 eV) changes only very slowly. In contrast, there is a strong change

in the density of holes around 1.4 eV below the Fermi energy. It is the spin flip of these minority holes that leads to the demagnetization of the material in the present model. The faster dynamics of the holes compared to the excited electrons are due to the difference in the density of states, cf. Fig. 2(a), which is considerably higher below the Fermi energy than above, so that in this energy region there is a larger scattering phase space. In addition, in that energy region there are "spin hot spots," i.e., points in the Brillouin zone where the states are completely spin-mixed. Their presence also contributes to spin-flip scattering processes.[29]

C. Qualitative considerations

As we saw from the results of the last section that electron-phonon scattering alone cannot explain the experimentally observed demagnetization, the next important step seems to be to extend the existing model to other scattering mechanisms, e.g., electron-electron or electron-impurity scattering. However, we argue that their inclusion is not likely to qualitatively improve the description of a pronounced ultrafast demagnetization, if one retains the limitation that the model contain only scattering, i.e., the redistribution of carriers in a fixed band structure. The argument is based on the observation that demagnetization in a fixed band structure involves a transfer of occupation from majority to minority electron states or minority to majority hole states. Since, roughly speaking, the exchange splitting shifts the energy of (single-particle) minority states up compared to majority states, a redistribution process needs energy, which can only be supplied by the exciting laser pulse.

One can make this observation quantitative by finding the minimal magnetization that the material can attain given a fixed amount of deposited energy ΔE. This leads to a linear
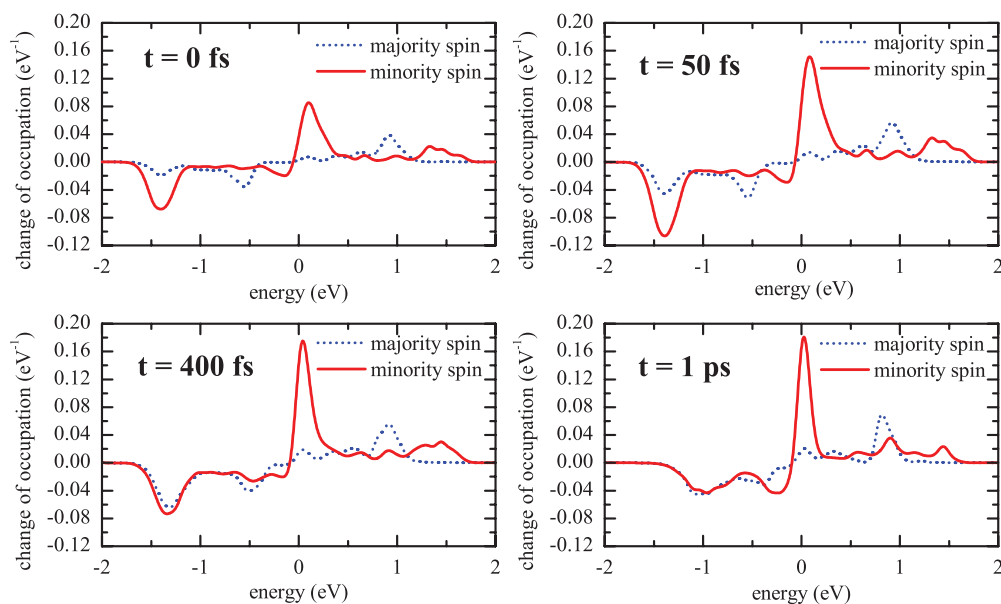

FIG. 5. (Color online) Energy- and spin-resolved occupation changes ΔN_σ at different times for nickel, as shown in Fig. 4, including the spin-orbit coupling in the electron-phonon matrix element. The representation is in analogy to the one for the optical excitation [Figs. 2(b) and 2(c)].
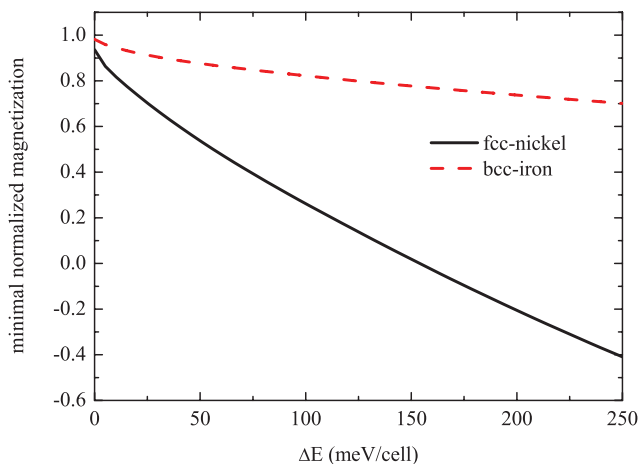
FIG. 6. (Color online) Theoretical limit for the minimal magnetization achievable by a pure redistribution in a fixed band structure for a range of deposited energies ΔE.

optimization problem

$$\min_{\{n_{\vec{k}}^{\mu}:0\leqslant n_{\vec{k}}^{\mu}\leqslant 1\}} \sum_{\vec{k}}\sum_{\mu} n_{\vec{k}}^{\mu} \langle S_z \rangle_{\vec{k}}^{\mu} \tag{29}$$

with the following constraints:

$$\sum_{\vec{k}}\sum_{\mu} n_{\vec{k}}^{\mu} = N_{\text{eq}}, \tag{30a}$$

$$\sum_{\vec{k}}\sum_{\mu} n_{\vec{k}}^{\mu} \epsilon_{\vec{k}}^{\mu} \leqslant E_{\text{eq}} + \Delta E. \tag{30b}$$

Here N_{eq} denotes the total number of carriers and E_{eq} the total energy of the system in equilibrium, i.e., before the arrival of the laser pulse. As before, the contribution from orbital angular momentum to the total magnetization is neglected. We solve this problem with the *ab initio* results at hand for a range of deposited energies ΔE, and show the results in Fig. 6. Note that we present the normalized magnetization, i.e., the minimum obtained from the solution of Eq. (29) divided by the equilibrium magnetization because this value can be readily compared to the demagnetization measured in an experiment. These values represent the minimal magnetization for a carrier distribution in the fixed (equilibrium) band structure given the deposited energy. It holds for all scattering mechanisms that could be creating this distribution provided that they either conserve energy (such as electron-electron scattering) or lead to a loss of energy by transferring it to other systems (such as electron-phonon scattering).

By comparing the experimental demagnetization with the calculated minimal magnetization at the amount of energy deposited in experiment one can see whether the experimental results can, in principle, be explained in terms of scattering alone. This comparison turns out to be not so easy as quite a lot of parameters (e.g., the spot size, absorption, and reflectivity) are necessary for the estimate of the deposited energy from the measured laser intensity and some of them are known only with a considerable uncertainty. That is why we chose to estimate the deposited laser energy directly from the measured magnetization dynamics. This is possible if one relies on two assumptions:

(1) At about 5 ps after the laser excitation the scattering processes have locally thermalized the material, so that the initial nonequilibrium dynamics has evolved into a quasiequilibrium dynamics, in which the magnetization at that time can be characterized by the temperature dependence of the magnetization in the ferromagnet $M(t \approx 5 \text{ ps}) = M(T)$ where $T = T(t \approx 5 \text{ ps})$.

(2) The coupling to the substrate and other losses are so weak that almost all of the energy deposited by the laser is still in the material at that point ($t \approx 5$ ps). However, it has been evenly distributed among the inner degrees of freedom.

These assumptions are consistent with interpretations of measured data by Koopmans *et al.*[30] and seem to be especially well fulfilled for measurements on thin films. They can now be used to extract the deposited energy from the measured magnetization at 5 ps, and to read off the corresponding achievable minimum magnetization from Fig. 6. This can be compared with the "quenched" magnetization reached in the same measurement. In typical data for nickel[31] and iron[32] at high intensities we find for the normalized magnetization after thermalization values of $M_{\text{Ni}}(5 \text{ ps}) = 0.1$ and $M_{\text{Fe}}(5 \text{ ps}) = 0.8$. Using the equilibrium temperature dependence of the magnetization $M(T)$, we conclude that the temperature after local thermalization is about 625 K for nickel and about 800 K for iron, respectively. As we assume an even distribution among the material's degrees of freedom, we can calculate the deposited energy as an integral over the heat capacity $C_{\text{p}}(T)$:

$$\Delta E = \int_{300 \text{ K}}^{T(5 \text{ ps})} dT \, C_{\text{p}}(T), \tag{31}$$

which we solved using experimental data for $C_{\text{p}}(T)$,[33] yielding $\Delta E(\text{Ni}) = 100$ meV/cell and $\Delta E(\text{Fe}) = 160$ meV/cell. For these energies, Fig. 6 yields 0.26 and 0.77 as minimal achievable magnetizations for nickel and iron, respectively. These values should be compared to the experimentally observed quenched magnetizations of 0.1 for nickel and 0.7 for iron. As the experimentally measured minima only slightly violate the theoretical bounds, one could be inclined to conclude that this argument does not rule out a demagnetization on the basis of pure redistribution in a fixed band structure. That view changes, however, if one looks at the corresponding distribution functions that are necessary to attain the theoretical magnetization minima. The one for nickel is shown in Fig. 7(a) and should be compared to the distribution that is created by pure optical excitation [Fig. 7(b)]. As discussed before, the optically excited distribution is the starting point for all scattering processes and we would expect these to bring the system back to a Fermi-Dirac distribution (at a higher temperature), which is also displayed in the figure. It is not at all likely that in the course of this process there will be an intermediate state that has a distribution that is anywhere close to the one shown in Fig. 7(a) for two reasons: First, for a magnetization close to the theoretical limit a highly "ordered" distribution is necessary, which is unlikely to be reached by random scattering processes. Second, the state shown in Fig. 7(a) lies very far off from the direct continuous transition from the distribution in Fig. 7(b) to the equilibrium distribution, both in terms of a simple relaxation time approximation and if one considers a quasielastic process,
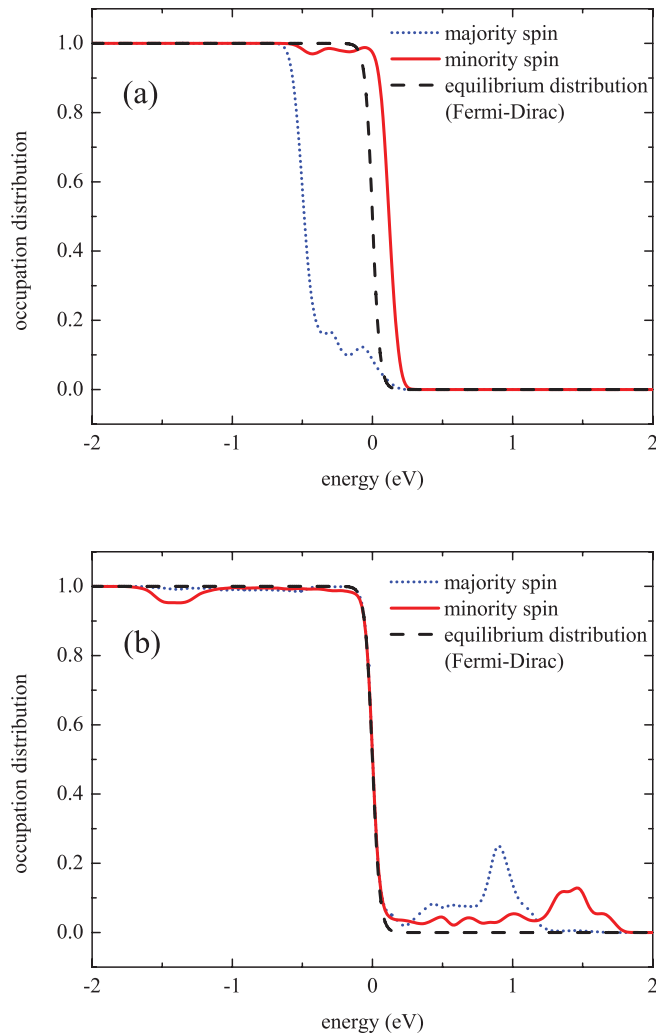
FIG. 7. (Color online) Energy- and spin-resolved occupation distributions for nickel. (a) shows the distributions that is necessary to attain the minimal magnetization for $\Delta E = 100$ meV/cell while (b) shows a typical distribution that would be created by the optical excitation (this is a slightly different representation of the data shown in Fig. 2(b). Here we show the occupation distribution, which allows an easier comparison with the equilibrium distribution).

such as electron-phonon scattering, where we have a slow, but continuous energy relaxation of the exited carriers toward the Fermi energy where eventually nonequilibrium electrons and holes cancel out.

Even though this argument is not a rigorous, we find it convincing enough to draw the conclusion that scattering dynamics in a fixed band structure cannot explain the observed ultrafast demagnetization. We therefore believe that it is important to include dynamical changes in the "magnetic structure." It is conceivable that the band structure, i.e., the exchange splitting, changes during the demagnetization process. For instance, there are time-resolved photoemission experiments[34] that point to a collapse of the magnetic exchange splitting for the Ni 3d valence states with a time constant of about 300 fs. We stress that our arguments above apply to extended systems without disorder. There may also be contributions that reduce the magnetization due to a finite thickness of the film, e.g., by superdiffusive transport of carriers out of the film into the substrate, or if one considers finite systems where the "band structure" consists of discrete levels, so that coherent processes may play a much bigger role.

Finally, we would like to comment on the relation of our results to an earlier paper,[10] in which we computed electron-electron scattering dynamics in a fixed band structure with spin-orbit splitting and analyzed its contribution to ultrafast demagnetization in 3d ferromagnets. The present results make it seem likely that in Ref. [10] we overestimated the energy deposited by the excitation pulse and thus the magnetization quenching achievable by electron-electron scattering in a fixed band structure. Electron-electron scattering certainly plays an important role in the demagnetization process, but its quantitative assessment should be done using a dynamical calculation that includes a change in the "magnetic structure."

IV. CONCLUSIONS

The main objective of this paper was to analyze in detail the dynamics due to one of the proposed mechanisms for ultrafast demagnetization: the Elliott-Yafet process based on electron-phonon scattering. To this end, we carried out a numerical analysis without adjustable parameters including the laser excitation and the scattering dynamics on the level of Boltzmann scattering integrals. We evaluated the model for the elementary ferromagnets nickel and iron utilizing realistic band structures and matrix elements obtained from *ab initio* calculations. As in other studies,[10,14,16] we kept the band structure fixed. In this case, the computed demagnetization for realistic pump-laser intensities is smaller by almost a factor of 10 than what is observed in experiments. An additional argument shows that this bound for the achievable magnetization "quenching" is likely to hold as well for other scattering mechanisms, such as electron-electron or electron-impurity scattering. We interpret our numerical results that any microscopic model that tries to explain ultrafast demagnetization by scattering dynamics really should include a dynamical change of the magnetic structure. It seems that without the latter ingredient, the demagnetization process cannot be explained by an Elliott-Yafet-type mechanism alone.

APPENDIX: NUMERICAL METHOD

For the numerical solution of Eq. (1) we replace the energy δ function in the scattering rates, Eq. (4), by a Gaussian of finite width to allow a Brillouin-zone integration on the chosen grid of $\vec{k}$ points. The full width at half maximum of this broadened distribution is taken to be 15 meV for the DFT grid at hand, and convergence of the results with respect to grid size and distribution width was checked.

1. Reducing the dimensionality of the problem

Two simplifications help to reduce the numerical effort for the solution of Eq. (1). The first is based on the fact that only the states in a limited energy range around the Fermi energy will experience an occupation change in the course of the dynamics. Due to the structure of the equilibrium distribution,

$$\left(n_{\vec{k}}^{\mu}\right)_{\mathrm{eq}} = \frac{1}{e^{(\epsilon_{\vec{k}}^{\mu}-\mu)/k_B T_0}+1}, \qquad (A1)$$

the states far ($\geqslant 200$ meV for $T_0 = 300$ K) above the Fermi energy ($\mu \approx E_F$) will be empty while those far below the Fermi energy will be fully occupied. As the incoming laser pulse will only cause resonant transitions between occupied and unoccupied states, the occupation change due to the optical excitation is limited to an energy range around the Fermi energy. This is clearly seen in the energy resolved occupation change due to the optical excitation in Fig. 2. States far away from the Fermi energy ($|\epsilon_{\vec{k}}^{\mu} - E_F| \gg E_{\mathrm{las}}$) remain at their equilibrium values. As the electron-phonon scattering transfers only small amounts of energy in each scattering process, the occupation of these states is not influenced by the following scattering dynamics either. That is why one can safely assume the occupation of these states to remain constant in time. Only states in an energy range $|\epsilon_{\vec{k}}^{\mu} - E_F| \leqslant \delta E$ are actually included in the dynamical calculation of the occupation numbers. So, for each $\vec{k}$ point, we only include the subset of bands $n_{\vec{k}}^{\mu_j}$ into the dynamical calculation that fall in the chosen energy range δE. For the calculations including only the optical excitation in Sec. III A we took δE to be 5 eV, but for the photon energy under investigation (1.55 eV) a much smaller range actually suffices. We therefore reduced it to 2 eV for the calculations including scattering in Sec. III B.

The second simplification can be made due to the crystal symmetries of the materials under investigation. These symmetries imply that the wave functions of two states at different $\vec{k}$ points that are related by a crystal symmetry operation are also connected by the same symmetry operation. From that one can deduce that the modulus of an electron-phonon matrix element between two states does not change if one applies a crystal symmetry operation on the initial and the final state. In other words, electron-phonon scattering will not break the symmetry of an occupation distribution that has the same symmetry as the crystal (e.g., the thermal distribution before optical excitation). The optical excitation could break that symmetry as it involves the scalar product with an external electric field. In our paper, we restrict ourselves to the description of the typical experimental case where the laser field is parallel to the material magnetization so that the symmetry of the occupation distribution is not broken by the optical excitation. In this case, it is not necessary to compute all occupation numbers $n_{\vec{k}}^{\mu}$. Rather, all information about the occupation distribution is contained in any subset $\{\vec{k}_j\}$ of $\vec{k}$ points, which constitutes an irreducible wedge of the Brillouin zone.

2. Numerical evaluation

With these two simplifications we are left with a subset of occupation numbers n_j, which need to be calculated dynamically. Here $j = (\vec{k}_j, \mu_j)$ denotes a multi-index that includes the $\vec{k}$ point as well as the band index of the state. With the help of this notation, Eq. (1) can be reformulated to yield

$$\frac{\partial n_j}{\partial t} = \left.\frac{\partial n_j}{\partial t}\right|_{\mathrm{opt}} + \left.\frac{\partial n_j}{\partial t}\right|_{\mathrm{e-p}}$$

$$= |\vec{E}(t)|^2 \sum_i \mathbf{B}_{ji}^{\mathrm{opt}} n_i$$

$$+ \sum_i \left(n_j \mathbf{A}_{ji}^{\mathrm{e-p}}(1-n_i) - (1-n_j)\mathbf{A}_{ij}^{\mathrm{e-p}} n_i\right), \quad (A2)$$

where all n_j-independent quantities are contained in the constant matrices $\mathbf{A}^{\mathrm{e-p}}$ and $\mathbf{B}^{\mathrm{opt}}$, which can be precomputed for the chosen set of states. Interpreting the occupation numbers n_j as a vector $\vec{n}$ we can alternatively write this as

$$\frac{\partial}{\partial t}\vec{n} = |\vec{E}(t)|^2 \mathbf{B}^{\mathrm{opt}}\vec{n}$$

$$+ \mathrm{diag}(\vec{n})\mathbf{A}^{\mathrm{e-p}}(\vec{1} - \vec{n})$$

$$- \mathrm{diag}(\vec{1} - \vec{n})(\mathbf{A}^{\mathrm{e-p}})^T\vec{n}, \qquad (A3)$$

where $\mathrm{diag}(\vec{n})$ is a matrix with the occupation numbers on the diagonal. $\vec{1}$ denotes a vector with all entries set to 1. In the form of Eq. (A3) the differential equation is especially well suited for a numerical evaluation. We used a MATLAB algorithm[35] for the solution.

*hcsch@physik.uni-kl.de

[1] E. Beaurepaire, J.-C. Merle, A. Daunois, and J.-Y. Bigot, Phys. Rev. Lett. **76**, 4250 (1996).

[2] B. Koopmans, G. Malinowski, F. Dalla Longa, D. Steiauf, M. Fähnle, T. Roth, M. Cinchetti, and M. Aeschlimann, Nat. Mater. **9**, 259 (2010).

[3] C. Stamm, T. Kachel, N. Pontius, R. Mitzner, T. Quast, K. Holldack, S. Khan, C. Lupulescu, E. F. Aziz, M. Wietstruk, H. A. Dürr, and W. Eberhardt, Nat. Mater. **6**, 740 (2007).

[4] K. Carva, D. Legut, and P. M. Oppeneer, Europhys. Lett. **86**, 57002 (2009).

[5] E. Carpene, E. Mancini, C. Dallera, M. Brenna, E. Puppin, and S. De Silvestri, Phys. Rev. B **78**, 174422 (2008).

[6] G. P. Zhang and W. Hübner, Phys. Rev. Lett. **85**, 3025 (2000).

[7] G. P. Zhang, Y. Bai, and T. F. George, Phys. Rev. B **80**, 214415 (2009).

[8] G. Lefkidis and W. Hübner, J. Magn. Magn. Mater. **321**, 979 (2009).

[9] U. Atxitia, O. Chubykalo-Fesenko, J. Walowski, A. Mann, and M. Münzenberg, Phys. Rev. B **81**, 174401 (2010).

[10] M. Krauß, T. Roth, S. Alebrand, D. Steil, M. Cinchetti, M. Aeschlimann, and H. C. Schneider, Phys. Rev. B **80**, 180407 (2009).

[11] D. Steil, S. Alebrand, T. Roth, M. Krauß, T. Kubota, M. Oogane, Y. Ando, H. C. Schneider, M. Aeschlimann, and M. Cinchetti, Phys. Rev. Lett. **105**, 217202 (2010).

[12]B. Koopmans, J. J. M. Ruigrok, F. Dalla Longa, and W. J. M. de Jonge, Phys. Rev. Lett. **95**, 267207 (2005).

[13]J. Walowski, G. Müller, M. Djordjevic, M. Münzenberg, M. Kläui, C. A. F. Vaz, and J. A. C. Bland, Phys. Rev. Lett. **101**, 237401 (2008).

[14]D. Steiauf and M. Fähnle, Phys. Rev. B **79**, 140401 (2009).

[15]D. Steiauf, C. Illg, and M. Fähnle, J. Magn. Magn. Mater. **322**, L5 (2010).

[16]K. Carva, M. Battiato, and P. M. Oppeneer, Phys. Rev. Lett. **107**, 207201 (2011).

[17]M. Battiato, K. Carva, and P. M. Oppeneer, Phys. Rev. Lett. **105**, 027203 (2010).

[18]A. R. Williams, J. Kübler, and C. D. Gelatt Jr., Phys. Rev. B **19**, 6094 (1979).

[19]J. Kübler, *Theory of Itinerant Electron Magnetism* (Oxford University Press, New York, 2000).

[20]V. Eyert, *The Augmented Spherical Wave Method*, Lecture Notes in Physics, No. 719 (Springer, Berlin, Heidelberg, 2007).

[21]G. Grimvall, *The Electron-Phonon Interaction in Metals* (North-Holland, Amsterdam, 1981).

[22]Y. Yafet, in *Solid State Physics*, edited by F. Seitz and D. Turnbull (Academic Press Inc., New York, 1963), Vol. 14.

[23]P. M. Oppeneer, T. Maurer, J. Sticht, and J. Kübler, Phys. Rev. B **45**, 10924 (1992).

[24]*American Institute of Physics Handbook*, edited by D. E. Gray, 3rd ed. (McGraw-Hill, New York, 1972).

[25]P. Giannozzi, S. Baroni, N. Bonini, M. Calandra, R. Car, C. Cavazzoni, D. Ceresoli, G. L. Chiarotti, M. Cococcioni, I. Dabo, A. Dal Corso, S. de Gironcoli, S. Fabris, G. Fratesi, R. Gebauer, U. Gerstmann, C. Gougoussis, A. Kokalj, M. Lazzeri, L. Martin-Samos, N. Marzari, F. Mauri, R. Mazzarello, S. Paolini, A. Pasquarello, L. Paulatto, C. Sbraccia, S. Scandolo, G. Sclauzero, A. P. Seitsonen, A. Smogunov, P. Umari, and R. M. Wentzcovitch, J. Phys.: Condens. Matter **21**, 395502 (2009).

[26]A. Dal Corso and S. de Gironcoli, Phys. Rev. B **62**, 273 (2000).

[27]P. B. Johnson and R. Christy, Phys. Rev. B **9**, 5056 (1974).

[28]M. Djordjevic, M. Lüttich, P. Moschkau, P. Guderian, T. Kampfrath, R. G. Ulbrich, M. Münzenberg, W. Felsch, and J. S. Moodera, Phys. Status Solidi C **3**, 1347 (2006).

[29]J. Fabian and S. Das Sarma, Phys. Rev. Lett. **81**, 5624 (1998).

[30]B. Koopmans, M. van Kampen, J. T. Kohlhepp, and W. J. M. de Jonge, Phys. Rev. Lett. **85**, 844 (2000).

[31]Measurements[2] on Ni (15 nm) film with 5.0 mJ/cm^2.

[32]Measurements[5] on Fe (7 nm) film with 6.0 mJ/cm^2.

[33] Landolt-Börnstein, *Magnetic Properties of Metals: III/19A*, edited by H. P. J. Wijn (Springer, Berlin, Heidelberg, 1986).

[34]H.-S. Rhie, H. A. Dürr, and W. Eberhardt, Phys. Rev. Lett. **90**, 247201 (2003).

[35]L. F. Shampine and M. W. Reichelt, SIAM J. Sci. Comput. **18**, 1 (1997).